Iranian Research Organization for Science and Technology (IROST)

# Fabrication and optimization of superhydrophobic ZnO-SA/PVC/PVP nanocomposite membrane distillation for highly saline RO brine recovery

Ehsan Kiyani Aliabadi[1], Abdolreaza Samimi[1,2], Davood Mohebbi-Kalhori[1,2], Razieh Beigmoradi[2,3]✉

[1] Department of Chemical Engineering, University of Sistan and Baluchestan, Zahedan, Iran
[2] Innovation Center for Membrane Technology (ICMT), University of Sistan and Baluchestan, Zahedan, Iran
[3] Department of Chemical Engineering, Faculty of Engineering, Ardakan University, Ardakan, Iran

## HIGHLIGHTS

• ZnO-SA nanoparticles were used to modify PVC/PVP composite membranes.

• Taguchi method was used to determine the optimal conditions for preparing PVC/PVP membranes.

• The super-hydrophobicity of one membrane was optimized.

## GRAPHICAL ABSTRACT
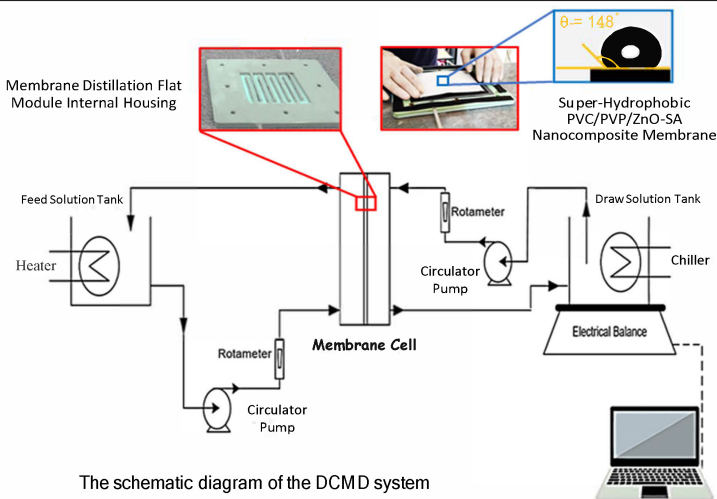


The schematic diagram of the DCMD system

## ARTICLE INFO

## ABSTRACT

The induced phase separation method was used to fabricate polyvinyl chloride (PVC) flat sheets for membrane distillation (MD) of RO brine feed by using dimethylformamide (DMF) and water as solvent and nonsolvent, respectively. Polyvinylpyrrolidone (PVP) and zinc oxide (ZnO) nanoparticles were utilized to improve the membrane structure and modify pore surfaces. The Taguchi experimental design approach was employed to investigate the impacts of concentrations of PVP and ZnO nanoparticles on the membrane's structural characteristics and performance. SEM, XRD, and FT-IR were used to characterize the surface and cross-sectional morphology, as well as the presence of crystalline phases and cross-linked organic groups, respectively. The water contact angle was measured to determine the wettability of the surface membrane and the impact of ZnO nanoparticles on its hydrophobicity. The membrane synthesis and MD process parameters were optimized for a Persian Gulf feed brine to obtain a maximum contact angle of 148°, under 80 °C and 12 L.min$^{-1}$ circulating feed water, and resulted in high salt rejection (96.4%) and proper permeability water flux (4.2 L.m$^{-2}$h$^{-1}$).

✉ *Corresponding author: E-mail address:* beigmoradi@ardakan.ac.ir ; *Tel* : +9854-31136459 ; *Fax* : +9854-33447092

## 1. Introduction

With growing worldwide urbanization and the development of industries and agriculture, fresh water has become more critical than ever. Membrane technology is one of the most effective ways to treat water and wastewater. Membranes' low energy consumption and various operating conditions for producing different types of water are their most important features, making them more popular among water technologies [1-3]. Desalinating seawater with reverse osmosis (RO) membrane technology is one of the most common ways to provide high-quality drinking water. However, even though this is a highly efficient process, it has become one of the most problematic environmental processes due to its release of salty wastewater [4-6].

Research is currently being conducted on how to recover and reclaim more pure water from brine wastewater of RO units. These methods usually use biological methods [7], membrane distillation (MD) technology [8], and forward osmosis (FO) membranes [9-10].

Since MD membranes are hydrophobic, liquid molecules cannot penetrate, and only water vapor molecules pass through the membrane. The vapor molecules pass across the pores and are condensed/evacuated on the permeate side of the membrane as a result of partial vapor pressure difference [2,11-13]. A pump circulates a condensing fluid (usually pure water) across the permeate side of the membrane. In MD cells, water or volatile organic compounds evaporate at the hot liquid/vapor interface, pass through the pores, and condense inside the condensing cold fluid. Low-grade heat sources can be used due to low-temperature differences. A further advantage of this method is that it requires less hydraulic pressure and mechanical strength than other membrane-type methods. There are four types of membrane distillation configurations: direct contact membrane distillation (DCMD), vacuum membrane distillation (VMD), sweeping gas membrane distillation (SGMD), and thermostatic sweeping gas membrane distillation (TSGMD) [11].

Similar to other membrane technologies, MD technology's success in water purification depends on the membrane's geometry and structure. It is crucial that a membrane used in the MD process has a high degree of hydrophobicity, proper pore size distribution, low heat transfer coefficient, and high liquid entry pressure to prevent wetting [12]. MD membranes can be produced using hydrophobic polymers such as PTFE, PVDF, or PP. It is also possible to form superhydrophobic membranes by modifying the surface of the membrane or forming composites [13].

Various methods have been developed to construct hydrophobic membranes with suitable structures, but an economically viable and readily available membrane remains a long way off [14]. Furthermore, to the best of our authors' knowledge, the number of studies synthesizing super-hydrophobic nanocomposite membranes for MD desalination of highly saline brine is scanty.

In this study, polyvinyl chloride (PVC) flat sheet membranes were manufactured using a nonsolvent-induced phase separation (NIPS) technique. Dimethylformamide (DMF) and water were used as the solvent and nonsolvent, respectively. Polyvinylpyrrolidone (PVP) and zinc oxide nanoparticles (ZnO NPs) coated with stearic acid were used to improve membrane structure and modify pore surfaces. The Taguchi experimental design was employed to investigate the effects of parameters on membrane structure. This study investigated the influence of PVP and ZnO NP concentration on the final membrane structure, contact angle, and performance.

X-ray diffraction (XRD), scanning electron microscopy (SEM), and Fourier transform infrared spectroscopy (FT-IR) were used to characterize the membrane. Surface membrane wettability was measured as a function of the water contact angle, where the impact of the ZnO NPs was investigated. As part of the feed process, highly saline RO brine from the plant in the Persian Gulf Special Economic Zone (Bandar Abbas, Iran) was processed for further desalination.

## 2. Experimental

This study used PVC grade S7051 resin purchased from Bandar Imam Khomeini Petrochemical Company (Iran), DMF as a solvent, dehydrated zinc acetate, sodium hydroxide, polyvinylpyrrolidone (PVP), and stearic acid

purchased from Merck (Germany). The ethanol was obtained from Dr. Mojalali Company (Iran).

Zinc oxide was prepared by mixing zinc acetate dihydrate (0.5 M) with sodium hydroxide (1 M) at a 1:1 volume ratio. A 100 ºC hot plate was used to stir the mixed solution (600 rpm) for 1 h (Labeled ZnO-SA). As soon as the suspension was prepared, it was filtered, washed with dispersed water several times, and dried at 65 ºC for 24 h. A 50 mg.ml$^{-1}$ ethanol concentration was mixed with the solids, followed by 30 mg/ml stearic acid. After stirring for 60 min, the mixture was filtered and dried at room temperature (Labeled ZnO-SA NPs).

For the experiment, three concentrations of PVP solution, 0, 2, and 4 %w/w, as well as three concentrations of ZnO-SA NPs, 0, 2, and 4 %w/w, were chosen.

In order to fabricate flat sheet membranes with 13 %wt PVC, precise amounts of solvent were added, followed by PVP polymer added according to the concentrations stated. Using the Yaxun YX-3560 ultrasonic bath, ZnO-SA NPs were dispersed after the polymers were completely dissolved. A doctor blade with a 150 $\mu$m gap was used to cast polymer solutions on a glass plate, which were immediately immersed in deionized water as a nonsolvent to induce phase inversion. After being kept in a water bath for 10 min, all samples were dried in an atmosphere.

In order to measure the membrane's performance, an industrial brine from a desalination unit in Bandar Abbas City was used as saline feed. In this study, three temperatures of 40, 60, and 80 ºC were selected, along with two flow rates of 6 and 12 liters per minute (L.min$^{-1}$). The analytical characteristics of RO brine are summarized in Table 1. Pure water permeance and salt rejection were measured using an experimental DCMD setup constructed at the Sistan and Baluchestan University's Innovation Center for Membrane Technology (ICMT).

Fig. 1 shows the schematic diagram of the experimental setup. Using a feed pump (JOVTOP, JT-800 model), water brine from the RO unit was fed to the membrane module (Fig. 2). Excess flow was bypassed to maintain a constant feed flow rate. Membranes were placed in a fabricated module.

Using cooling water, the permeated water vapor was continuously condensed on the permeate side of the membrane

**Table 1.** Analytical specifications of this effluent of RO process treatment plant from the Persian Gulf Special Economic Zone.

| Parameter | The amount in the effluent | Unit |
|---|---|---|
| pH | 8.52 | - |
| EC | 89.4 | ds.m$^{-1}$ |
| TDS | 50064 | mg.L$^{-1}$ |
| TH | 15460 | mg.L$^{-1}$ as $CaCO_3$ |
| Ca | 3650 | mg.L$^{-1}$ as $CaCO_3$ |
| Mg | 11810 | mg.L$^{-1}$ as $CaCO_3$ |
| Phenolphthalein | 7.70 | mg.L$^{-1}$ as $CaCO_3$ |
| Methyl orange | 213 | mg.L$^{-1}$ as $CaCO_3$ |
| Turbidity | 2.30 | N.T.U |
| Color | 14.0 | T.C.U |
| $NH_4$ | 1.12 | mg.L$^{-1}$ |
| $NH_3$ | 5.33 | mg.L$^{-1}$ |
| $SiO_2$ | 85.0 | mg.L$^{-1}$ |
| $Fe^{3+}$ | 0.32 | mg.L$^{-1}$ |
| $Ca^{2+}$ | 440 | mg.L$^{-1}$ |
| $Mg^{2+}$ | 1506 | mg.L$^{-1}$ |
| $Na^+$ | 21170 | mg.L$^{-1}$ |
| $K^+$ | 53 | mg.L$^{-1}$ |
| Mn | 76.50 | mg.L$^{-1}$ |
| Cr | 1.89 | mg.L$^{-1}$ |
| Ni | 0.18 | mg.L$^{-1}$ |
| Ba | 1.25 | mg.L$^{-1}$ |
| Cu | 1.43 | mg.L$^{-1}$ |
| $PO_4^{3-}$ | 29 | mg.L$^{-1}$ |
| $SO_4^{2-}$ | 7200 | mg.L$^{-1}$ |
| $NO_3^-$ | 68 | mg.L$^{-1}$ |
| $NO_2^-$ | 0.5 | mg.L$^{-1}$ |
| $CO_3^-$ | 65 | mg.L$^{-1}$ |
| $HCO_3^-$ | 236 | mg.L$^{-1}$ |
| $F^-$ | 2.23 | mg.L$^{-1}$ |
| $Cl^-$ | 47546 | mg.L$^{-1}$ |
| $Al^{3+}$ | 0.19 | mg.L$^{-1}$ |

module. In a graduated tank, permeate was collected under steady-state conditions and weighed simultaneously to determine the flux of the membrane. A temperature controller with a heater was connected to maintain the temperature of the feed solution in the feed tank.
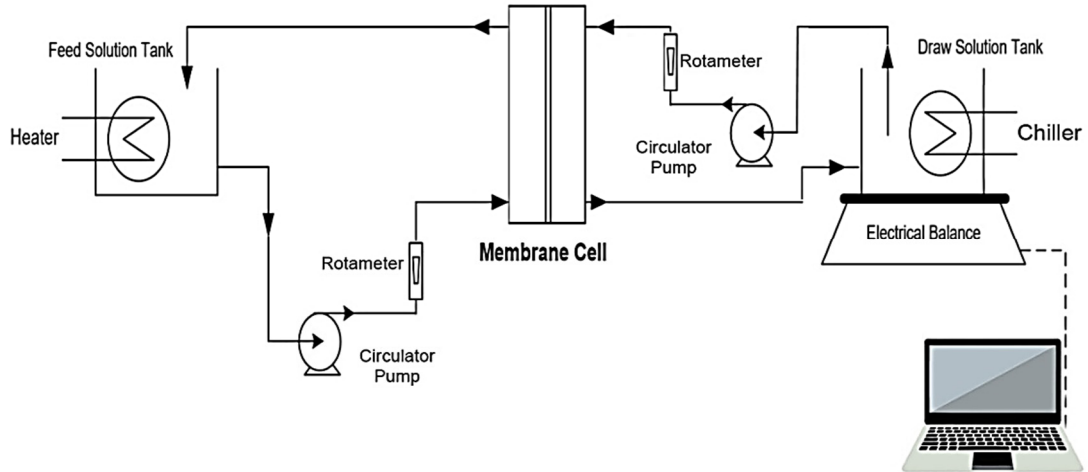
**Fig. 1.** The lab-scale DCMD schematic diagram.
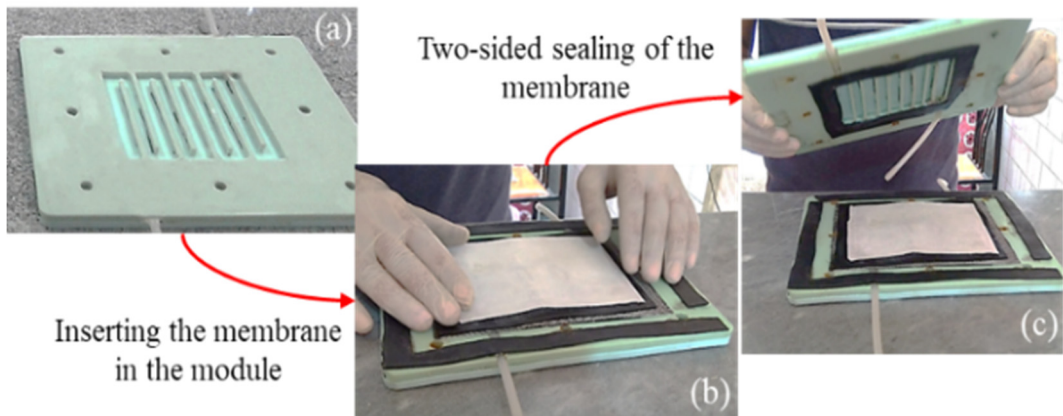


**Fig. 2.** (a) The designed module and (b)-(c) the assembly of the MD cell with a dimension of 13 cm × 15 cm.

The Pure water permeance through the PVC/PVP/ZnO-SA membrane was calculated according to Eq (1).

$$J = \frac{V}{At} \tag{1}$$

where $J$, $V$, $A$, and $t$ represent the permeate flux in L.m$^{-2}$.h$^{-1}$, volume (L), the effective membrane area (m$^2$), and the passage time of the liquid through the membrane (h), respectively [11-14].

The salt rejection ($R_s$%) was evaluated by calculating the concentrations of salts in the permeated water ($C_p$) and the feed ($C_f$) solutions using a conductance meter (CM-53, Japan) as follows [13-14].

$$R_s\% = \left(1 - \frac{c_p}{c_f}\right) \times 100 \tag{2}$$

SEM (JSM-7610FPlus, Japan) was used to determine the pore size distribution and to observe the surface and cross-sectional morphology of each membrane sample. The FT-IR (Shimadzu's IRTracer-100) and XRD (XRD-7000, Japan) spectra were employed to characterize the composition and crystalline phases.

A CA Meter (Iran) was used to measure the contact angle and wettability of the surface membranes. ImageJ (http://rsb.info.nih.gov/ij/download.html, National Institutes of Health, USA) was used to estimate the average pore size distribution. Thicknesses were measured using a digital gauge (accurate to 1 m, Asimeto, Japan). After at least three repetitions, average results were reported.

# 3. Results and discussion

## 3.1. Experimental design and statistical data analysis

In order to investigate the effect of two parameters, ZnO-SA NPs and PVP concentration, on the hydrophobicity of the membranes, the contact angle was considered as the response. Each membrane was tested at four different points, and the average contact angle was reported. Fig. 3 illustrates the average contact angle analysis images for all samples. Table 2 summarizes the results of each experiment.

A three-dimensional plot was generated by the software (Fig. 4) to help visualize the interaction between PVP, ZnO-SA NPs concentration on contact angle as the response. According to the figure, both parameters have an optimal value to maximize contact angle increase. ZnO-SA NPs are more effective than PVP in increasing the hydrophobicity of surface membranes. It occurs when the amount of ZnO-SA NPs is 2 wt%. Based on these results, the highest response increase occurs at 2 wt% of PVP concentration. Further analysis was performed for the membrane fabricated using test no. 16 as the optimal condition.

**Table 2.** Experimental layouts of an $L_{16}$ orthogonal array. Columns A indicates the number of factors at the levels, and B, the response, is the average contact angle.

| Run No. | Factor 2: (B) PVP (%wt) | Factor 1: (A) ZnO-SA (%wt) | Response: Average contact angle (°) |
|---|---|---|---|
| 1 | 0 | 0 | 98 |
| 2 | 2 | 0 | 82 |
| 3 | 4 | 2 | 127 |
| 4 | 4 | 4 | 120 |
| 5 | 2 | 4 | 129 |
| 6 | 4 | 2 | 133 |
| 7 | 4 | 0 | 73 |
| 8 | 2 | 2 | 146 |
| 9 | 0 | 0 | 90 |
| 10 | 0 | 4 | 127 |
| 11 | 2 | 2 | 145 |
| 12 | 2 | 2 | 146 |
| 13 | 0 | 0 | 87 |
| 14 | 2 | 4 | 133 |
| 15 | 0 | 2 | 142 |
| 16 | 2 | 2 | 148 |

## 3.2. Structural Analyses

### 3.2.1. SEM image analysis

A SEM image of the top surface of the nanocomposite membrane is shown in Fig. 5. The image shows a porous surface (Fig. 5(a)). In the zoomed image (Fig. 5(b)), the pore size was found to be approximately 0.2-0.4 $\mu$m with a circular shape.

Fig. 6(a) shows the cross-sectional morphologies. This membrane is expected to promote the development of fingers as a result of its creation using NIPS technology.

ZnO NPs dispersion was found to be homogeneous without defects across membrane morphology. There were, however, a few aggregates observed as reported in the literature [15-16].

A nanoparticle with a high surface area would reduce surface energy and enhance system stability (see zoomed image in Fig. 6(b)). These connected pores are considered very suitable conduits for pure vapor to pass through.

### 3.2.2. XRD analysis

Fig. 7 shows the XRD spectra of the nanocomposite membrane and ZnO nanoparticles. The XRD pattern of the membrane depicts a sharp peak centered at $2\theta = 5º$ and 27º (see Fig. 7(a)). A number of peaks are also observed at degrees 31.77º, 36.23º, 47.56º, and 56.61º, indicating that ZnO NPs embedded in membrane structures are highly crystalline. In the case of the PVP/PVC/ZnO-AS nanocomposite membrane, the new peaks at $2\theta$ are attributed to the (001), (002), (03), (004), and (005) planes of ZnO NPs (Fig. 7(b)). PVP/PVC/ZnO-AS nanocomposite membranes are prepared using uniformly dispersed NPs in polymer matrix without disrupting ZnO NP shapes. The PVP/PVC/ZnO-AS nanocomposite membrane exhibited sharp diffraction peaks, whereas ZnO NPs exhibit crystalline structure. As shown by the XRD pattern, PVC/PVP/ZnO-SA nanocomposites have low-intensity peaks compared to other PVC peaks [15,17], and the crystallinity of the nanocomposites has been reduced by the formation of cationic compounds with substituents and electron accepting groups. These results confirm nanoparticle interaction in PVC/PVP polymers. The XRD pattern

**Run #1: 98°**     **Run #2: 82°**     **Run #3: 127°**     **Run #4: 120°**

**Run #5: 129°**     **Run #6: 133°**     **Run #7: 73°**     **Run #8: 146°**

**Run #9:90°**     **Run #10: 127°**     **Run #11:145°**     **Run #12: 146°**

**Run #13:87°**     **Run #14: 133°**     **Run #15:142°**     **Run #16: 148°**
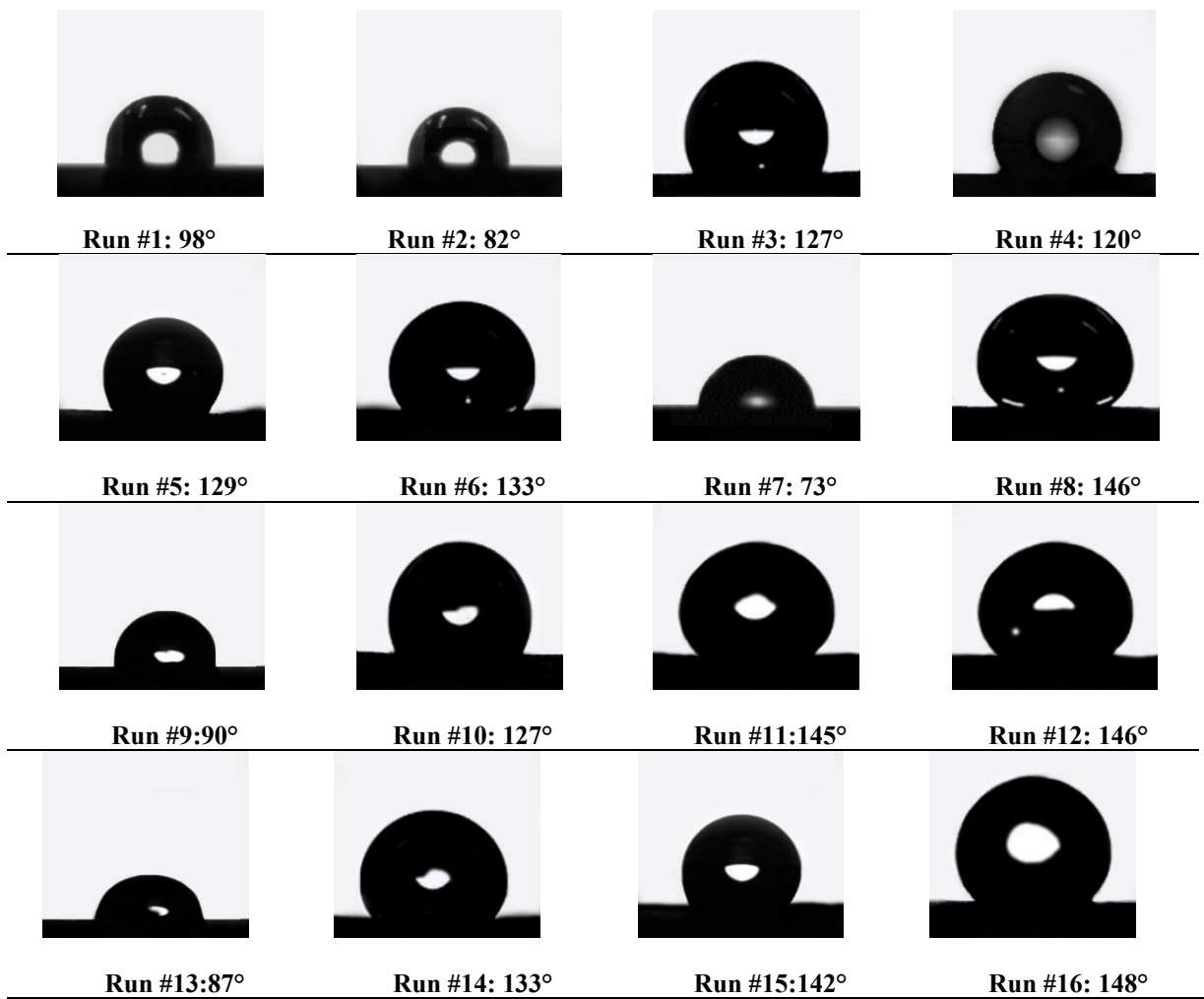
**Fig. 3.** The average contact angle of prepared membranes.
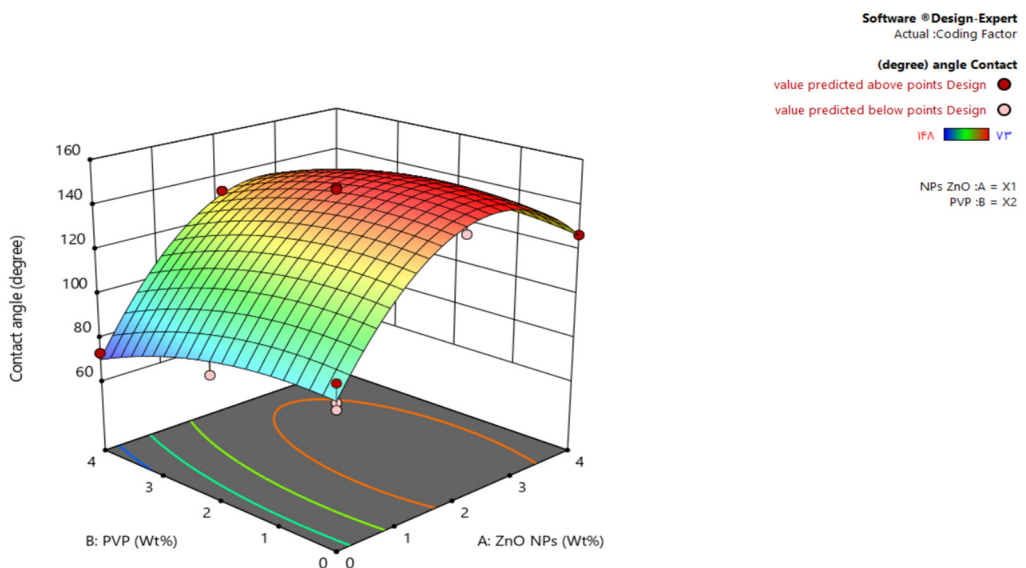


**Fig. 4**. A three-dimensional plot of two factors of the PVP, ZnO-SA NPs concentration and the contact angle as the response.
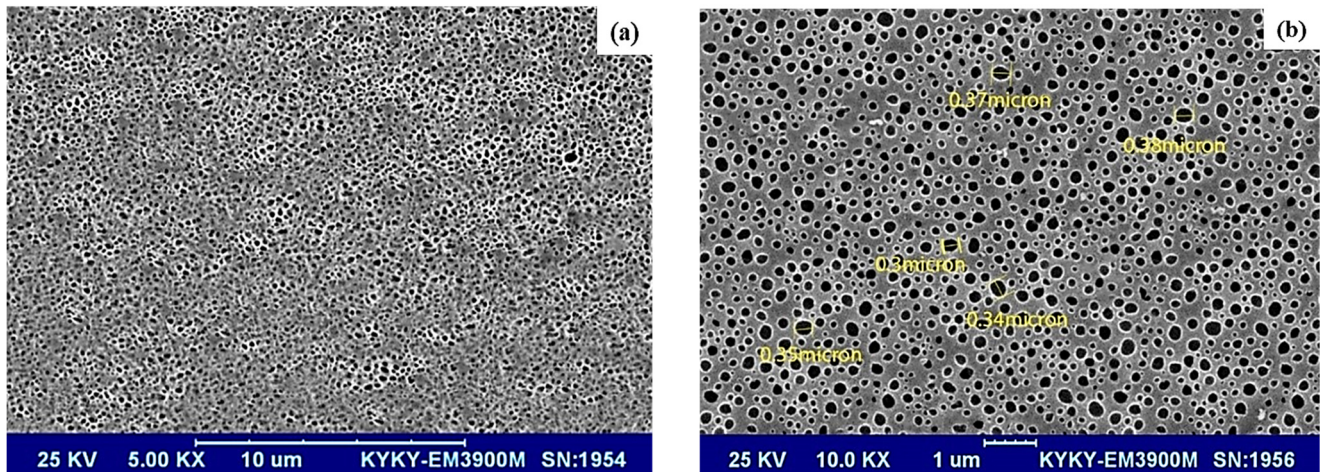
**Fig. 5**. (a) Surface SEM images of optimized membranes and (b) a high-resolution image for pore size estimation**.**
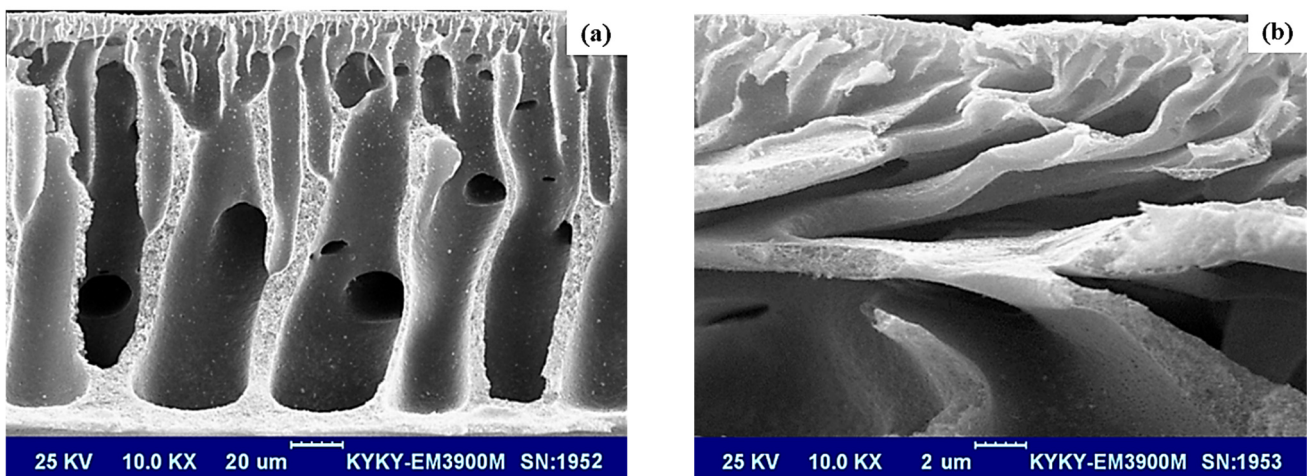


**Fig. 6.** (a) The cross-sectional SEM image of the nanocomposite membrane, and (b) a porous structure of the inside pores.

confirmed the formation of crystals, which matched exactly with JCPDS card no. 36–1451.

Nanoparticle size can be calculated using the Debye-Scherer formula as in Eq. (3) [15]. Here $\gamma$ is the wavelength of the X-ray (1.54 Å), $\theta$ is the Bragg diffraction angle, and $\beta$ is the peak width at half maximum. The peaks at 31.77º (001), 34.41º (002), and 36.23º (101) of the XRD spectrum correspond to 44, 45, and 55 nm, respectively.

$$D = \frac{0.9\gamma}{\beta \cos \theta} \tag{3}$$

### 3.2.3. FT-IR analysis

Fig. 8 shows the FT-IR spectrum of the membrane. FT-IR spectroscopy confirmed that fatty acid layers form on the surface when their carboxylate group interacts with ZnO.

This figure shows the FT-IR spectrum of a ZnO-SA superhydrophobic coating. Peaks at 2850 and 2920 cm$^{-1}$ correspond to the symmetric and asymmetric CH tensile states. Peaks at 1704 cm$^{-1}$ indicated unreacted acids. The asymmetric and symmetric bands attributed to COO− are attributed to about 1541 and 1466 cm$^{-1}$, respectively. Hence, it can be verified that the stearate ion with Zn$^{2+}$ appears to be COO−R. Thus, alkanoic acids chemically bonded to Zn$^{2+}$, resulting in an organic layer covering the microstructure surface of ZnO. The peak of ZnO-SA was observed at 418 cm$^{-1}$ [18-19].

Peak 1427 cm$^{-1}$ was assigned to the CH$_2$ bond in the PVC chain, peak 1650 cm$^{-1}$ to the C-O conformation, and peak 1374 cm$^{-1}$ to the C-H conformation in the PVP polymer. ZnO-SA embedded in the polymers shifts the transmission peak [18].

An interaction between ZnO-SA and polymers explained the displacement.
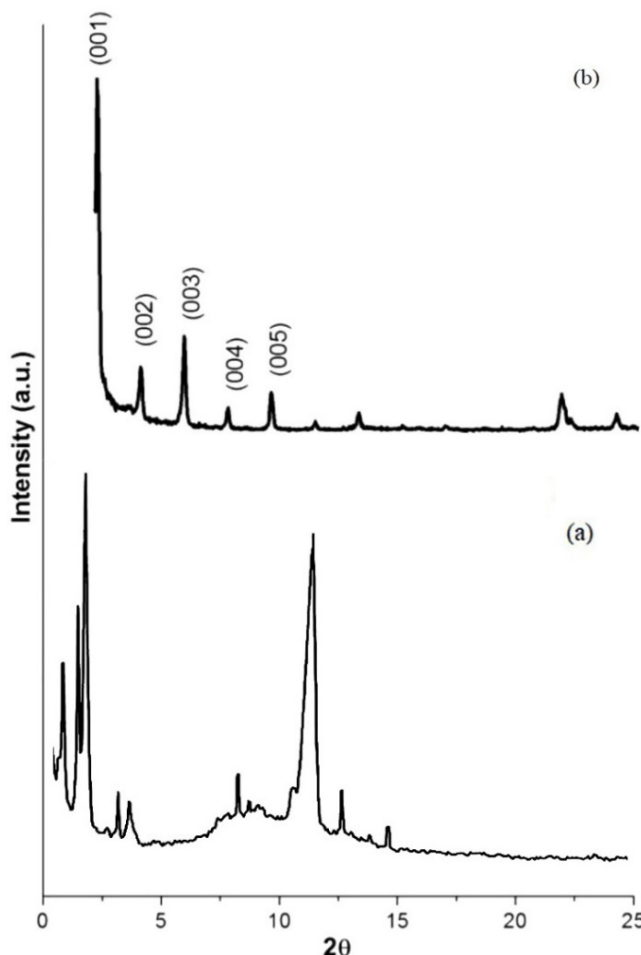


**Fig. 7.** (a) XRD spectra of the optimized membrane and (b) synthesized ZnO-SA.
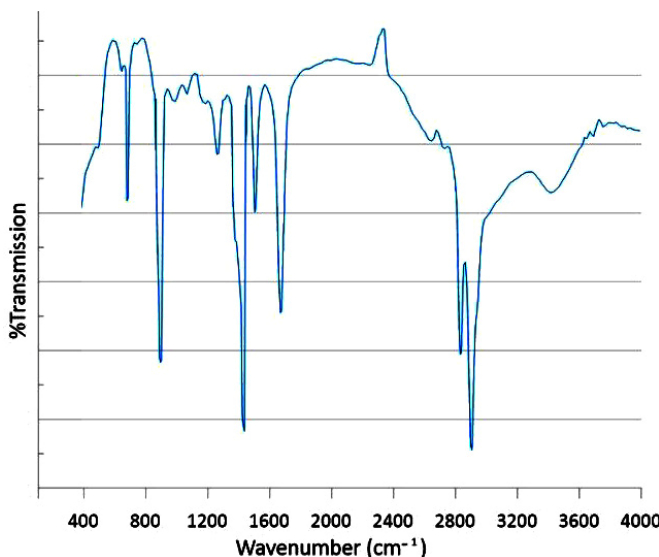


**Fig. 8**. FT-IR spectrum for the PVP/PVC/ZnO-AS nanocomposite membrane.

### *3.2.4. Dynamic water contact angle analysis*

Fig. 9 shows the dynamic water contact angle for the membrane at 0, 5, 10, 15, 20, 25 and 30 min. Upon exposure to water for 10 min, the sample's contact angle decreased, and after 30 min, it reached 45°, suggesting that water begins penetrating the membrane pores after 10 min, and after 30 min, it becomes permeable.
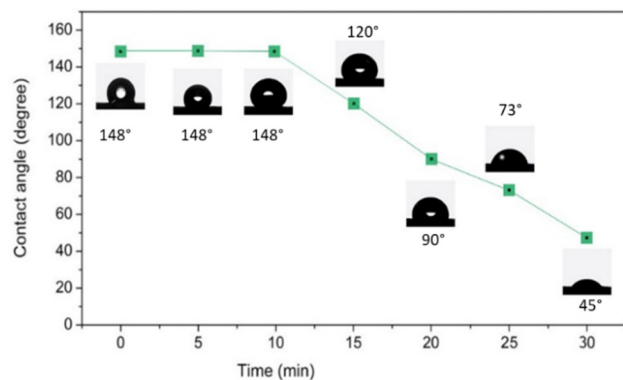


**Fig. 9.** Images of the dynamic water contact angle of the polymeric surface at different time points: 0, 5, 10, 15, 20, 25, and 30 min.

### 3.3. Performance analysis

Fig. 10 shows the water permeation flux of the membrane as a function of temperature and flow rate. Atmospheric pressure was used during the process, with a minimum water temperature difference of 25 °C on the membrane side.

According to Fig. 10, increasing the feed water flow rate and raising the feed temperature can increase permeability. When the temperature is 80 °C and the flow rate is 12 L.min$^{-1}$, the permeability is 4.2 kg.m$^{-2}$h$^{-1}$. Using the rejection formula (Eq. (2)), 96.4% of the salt of the feed was reduced by the membrane.

Similar results were obtained in similar studies, confirming the MD process' effectiveness in desalinating salty water. A hydrophobic polyvinylidene fluoride (PVDF) membrane was used in the work of Zhongsen Yan *et al.* to desalinate RO brine. According to their research, an MD membrane with a contact angle of 135° could reject 96.3% salinity. It was reported that the maximum permeability was around 8 L.m$^{-2}$h$^{-1}$ [20].
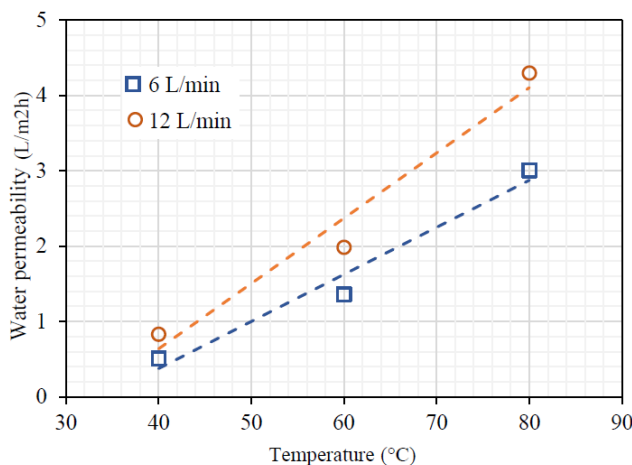
**Fig. 10.** The effect of temperature feed on the water permeability (○: 6 L.min⁻¹, □: 12 L.min⁻¹).

## 4. Conclusion

This work manufactured PVC flat sheet membranes for the DCMD process using non-solvent-induced phase separation methods. The membrane structure was improved, and pore surfaces were modified using PVP and ZnO nanoparticles covered in stearic acid. An experimental design based on Taguchi was utilized to study membrane characteristics and their effect on permeability flux, salt rejection, and membrane hydrophobicity. Compared with PVP, ZnO-SA NPs provide a greater maximum contact angle and hydrophobicity of surface membranes. The highest hydrophobicity was achieved with 2 %wt ZnO-SA NPs and 2 %wt PVP. The MD membrane demonstrated excellent desalination performance, with an ion rejection rate exceeding 95%. These results demonstrate that MD can be an effective and efficient method for recovering highly saline water and RO brine compared to other methods.

## Conflicts of interest

No potential conflict of interest was reported by the authors.

## References

[1] Abounahia, N. M., El-Sayed, A. M. A., Saleem, H., & Zaidi, S. J. (2023). An Overview on the Progress in Produced Water Desalination by Membrane-Based Technology. *Journal of Water Process Engineering*, *51*, 103479. https://doi.org/10.1016/j.jwpe.2022.103479

[2] Zhang, X., Koirala, R., Pramanik, B., Fan, L., Date, A., & Jegatheesan, V. (2023). Challenges and Advancements in Membrane Distillation Crystallization for Industrial Applications. *Environmental Research*, *234*, 116577. https://doi.org/10.1016/j.envres.2023.116577

[3] Korak, J. A., Mungan, A. L., & Watts, L. T. (2023). Critical Review of Waste Brine Management Strategies for Drinking Water Treatment Using Strong Base Ion Exchange. *Journal of Hazardous Materials*, *441*, 129473. https://doi.org/10.1016/j.jhazmat.2022.129473

[4] Tu, W. H., Zhao, Y., Chan, W. P., & Lisak, G. (2023). Reclaimed Seawater Discharge-Desalination Brine Treatment and Resource Recovery System. *Water Research*, *251*, 121096. https://doi.org/10.1016/j.watres.2023.121096

[5] Abid, M. B., Wahab, R. A., Salam, M. A., Moujdin, I. A., & Gzara, L. (2023). Desalination Technologies, Membrane Distillation, and Electrospinning, An Overview. *Heliyon*, *9*(2), e12801. https://doi.org/10.1016/j.heliyon.2023.e12810

[6] Pathak, N., Shon, H., Yu, H., Choo, Y., Naidu, G., Akther, N., & Han, D. S. (2023). Membrane Technology for Brine Management and Valuable Resource Recovery. In L. F. Dumée, M. Sadrzadeh & M. M. A. Shirazi (Eds.), *Green Membrane Technologies towards Environmental Sustainability* (pp. 415-441). Elsevier. https://doi.org/10.1016/B978-0-323-95165-4.00014-8

[7] Zhao, Z., Muylaert, K., & Vankelecom, I. F. (2023). Applying Membrane Technology in Microalgae Industry: A Comprehensive Review. *Renewable and Sustainable Energy Reviews*, *172*, 113041. https://doi.org/10.1016/j.rser.2022.113041

[8] Fontana, D., Forte, F., Pietrantonio, M., Pucciarmati, S., & Marcoaldi, C. (2023). Magnesium Recovery from Seawater Desalination Brines: A Technical Review. *Environment, Development and Sustainability*, *25*, 13733-13754.

https://doi.org/10.1007/s10668-022-02663-2

[9] Ibraheem, B. M., Aani, S. A., Alsarayreh, A. A., Alsalhy, Q. F., & Salih, I. K. (2023). Forward Osmosis Membrane: Review of Fabrication, Modification, Challenges and Potential. *Membranes*, *13*(4), 379. https://doi.org/10.3390/membranes13040379

[10] Abounahia, N., Ibrar, I., Kazwini, T., Altaee, A., Samal, A. K., Zaidi, S. J., & Hawari, A. H. (2023). Desalination by the Forward Osmosis: Advancement and Challenges. *Science of The Total Environment*, *886*, 163901.
https://doi.org/10.1016/j.scitotenv.2023.163901

[11] Tai, Z. S., Othman, M. H. D., Koo, K. N., & Jaafar, J. (2023). Critical Review on Membrane Designs for Enhanced Flux Performance in Membrane Distillation. *Desalination*, *553*, 116484.
https://doi.org/10.1016/j.desal.2023.116484

[12] Chang, H., Liu, B., Zhang, Z., Pawar, R., Yan, Z., Crittenden, J. C., & Vidic, R. D. (2020). A Critical Review of Membrane Wettability in Membrane Distillation from the Perspective of Interfacial Interactions. *Environmental Science & Technology*, *55*(3), 1395-1418.
https://doi.org/10.1021/acs.est.0c05454

[13] Kebria, M. R. S., & Rahimpour, A. (2020). Membrane Distillation: Basics, Advances, and Applications. *Advances in membrane technologies*. In A. Abdelrasoul (Ed.), IntechOpen.
https://doi.org/10.5772/intechopen.86952

[14] Ravi, J., Othman, M. H. D., Matsuura, T., Bilad, M. R. I., El-Badawy, T. H., & Aziz, F., *et al.* (2020). Polymeric Membranes for Desalination Using Membrane Distillation: A Review. *Desalination*, *490*, 114530.
https://doi.org/10.1016/j.desal.2020.114530

[15] Erdugan, B. M., Demirel, E., & Suvaci, E. (2022). Preparation and Characterization of Polyvinyl Chloride Membranes Decorated with Designed Novel Zinc Oxide Particles for Mitigating Uncontrollable Agglomeration. *Journal of Environmental Chemical Engineering*, *10*(5), 108388.
https://doi.org/10.1016/j.jece.2022.108388

[16] Mousa, S. A., Abdallah, H., & Khairy, S. A. (2023). Low-Cost Photocatalytic Membrane Modified with Green Heterojunction $TiO_2$/ZnO Nanoparticles Prepared from Waste. *Scientific Reports*, *13*(1), 22150.
https://doi.org/10.1038/s41598-023-49516-0

[17] Erdugan, B. M., Dadashov, S., Demirel, E., & Suvaci, E. (2021). Effect of Polymer Type on the Characteristics of ZnO Embedded Nanocomposite Membranes. *Desalination and Water Treatment*, *213*, 159-176. https://doi.org/10.5004/dwt.2021.26714

[18] Cai, W., Chen, H., Lin, J., Liu, Y., Wu, F., & Pu, X. (2023). Inorganic Nanoparticles-Modified Polyvinyl Chloride Separation Membrane and Enhanced Anti-Fouling Performance. *Surfaces and Interfaces*, *38*, 102885. https://doi.org/10.1016/j.surfin.2023.102885

[19] Ali, H., Al-Kadhemy, M. F. H., & Saeed, A. A. (2022). Physical Properties and Transmitted Sunlight of Polyvinyl Chloride/ZnO Nanocomposites Films. *Journal of Kufa-Physics*, *14*(02), 16-28.
https://doi.org/10.31257/2018/JKP/2022/140203

[20] Xu, Y., Yang, Y., Sun, M., Fan, X., Song, C., Tao, P., & Shao, M. (2021). High-Performance Desalination of High-Salinity Reverse Osmosis Brine by Direct Contact Membrane Distillation Using Superhydrophobic Membranes. *Journal of Applied Polymer Science*, *138*(5), 49768.
https://doi.org/10.1002/app.49768

**Additional information**

Correspondence and requests for materials should be addressed to R. Beigmoradi.